Astron. Astrophys. 362, 42–52 (2000)

ASTRONOMY AND ASTROPHYSICS

Complex molecular gas structure in the Medusa merger

S. Aalto[1] **and S. Hüttemeister**[2]

[1] Onsala Rymdobservatorium, 43992 Onsala, Sweden
[2] Radioastronomisches Institut der Universität Bonn, Auf dem Hügel 71, 53121 Bonn, Germany

Received 23 December 1999 / Accepted 3 August 2000

Abstract. High resolution OVRO aperture synthesis maps of the ^{12}CO 1–0 emission in the "Medusa" galaxy merger (NGC 4194) reveal the molecular emission being surprisingly extended. The ^{12}CO emission is distributed on a total scale of 25″ (4.7 kpc) — despite the apparent advanced stage of the merger. The complex, striking ^{12}CO morphology occupies mainly the center and the north-eastern part of the main optical body. The extended ^{12}CO flux is tracing two prominent dust lanes: one which is crossing the central region at right angle (with respect to the optical major axis) and a second which curves to the north-east and then into the beginning of the northern tidal tail.

The bulk of the ^{12}CO emission (67%) can be found in a complex starburst region encompassing the central 2 kpc. The molecular gas is distributed in five major emission regions of typical size 300 pc. About 15% of the total ^{12}CO flux is found in a bright region 1.″5 south of the radio continuum nucleus. We suggest that this region together with the kpc sized central starburst is being fueled by gas flows along the central dust lane. We discuss the merger history of NGC 4194 and suggest that it may be the result of a early-type/spiral merger with a shell emerging to the south of the center.

The total molecular mass in the system is estimated to be at most 2×10^9 M$_\odot$, depending on which ^{12}CO - H_2 conversion factor is applicable. The high ^{12}CO/^{13}CO 1–0 intensity ratio, ≈ 20, indicates highly excited physical conditions in the interstellar medium showing that the starburst has a big impact on its surrounding ISM. At the current rate of star formation, the gas will be consumed within 40 million years.

Key words: galaxies: evolution – galaxies: individual: NGC 4194 – galaxies: ISM – galaxies: starburst – radio lines: galaxies – radio lines: ISM

1. Introduction

The Medusa merger, NGC 4194, (Table 1; Fig. 1) belongs to a class of lower luminosity ($L_{\rm FIR} = 8.5 \times 10^{10}$ L$_\odot$ at D=39 Mpc) mergers, an order of magnitude fainter than well known Ultra Luminous Galaxies (ULIRGs ($L_{\rm FIR} \gtrsim 10^{12}$ L$_\odot$)) such as Arp 220, but with an extended region of intense star formation (Prestwhich et al. 1994; Armus et al. 1990). As the name indicates, the morphology of the Medusa merger is as spectacular as that of the brighter objects. The "hair" or "tentacles" are a patchy tidal tail stretching out 60″ (11.3 kpc) north of the main body, which appears twisted. There also is a sharp, curved feature (and a very faint tail) to the south.

NGC 4194 has been mapped in ^{12}CO 1-0 and 2-1 with a single dish telescope by Casoli et al. (1992) and detected in the more highly excited ^{12}CO 3-2 line by Devereux et al. (1994). It is one of the handful known mergers (e.g. Arp 220, IC 694, NGC 6240) with unusually high ^{12}CO/^{13}CO 1–0 intensity ratios, $\mathcal{R}$ >20 (e.g. Aalto et al. 1991b; Casoli et al. 1992). In contrast, the majority of large galaxies exhibit $\mathcal{R}$ in the range 5 — 15 (e.g. Aalto et al. 1995). One feature these HR (High Ratio) mergers have in common is a high FIR $f(60\,\mu{\rm m})/f(100\,\mu{\rm m})$ flux ratio $\gtrsim 0.8$ – which likely is an indication of a high dust temperature (e.g. Aalto et al. 1991a, 1991b). High resolution ^{12}CO maps of several luminous ($L_{\rm IR} \gtrsim 10^{11}$ L$_\odot$) HR mergers reveal that nearly all the molecular gas is concentrated within a few hundred parsecs of the center (e.g. Scoville et al. 1989; Bryant & Scoville 1996; Downes & Solomon 1998).

The resulting large central surface densities require high pressures in hydrostatic equilibrium and the molecular ISM becomes highly turbulent. Large turbulent line widths in molecular clouds will result in reduced optical depths in the ^{12}CO 1–0 line and the ^{12}CO/^{13}CO 1–0 line ratio will be elevated compared to the optically thick ratio (for a discussion see Aalto et al. 1995). So for the luminous HR mergers this could be one important mechanism behind the large observed ^{12}CO/^{13}CO line ratios (Aalto et al. 1995), aside from the additional effect from large kinetic temperatures. Will the lower luminosity HR galaxy NGC 4194 also follow this pattern of a compact nuclear starburst, or will an extended ^{12}CO distribution require a different dominant mechanism behind the elevated $\mathcal{R}$?

Most of the high resolution imaging effort of ^{12}CO in mergers has been directed toward the ULIRGs and not much is known, statistically, of the more modest luminosity merging galaxies. Apart from addressing the question of the compactness of the ^{12}CO emission in an HR merger, a ^{12}CO image of NGC 4194 will improve the statistics of the ^{12}CO distribution in moderate luminosity mergers.

The elevated values of $\mathcal{R}$ in hot dust mergers have also been interpreted as a global underabundance in ^{13}CO with respect

Send offprint requests to: S. Aalto (susanne@oso.chalmers.se)

Table 1. Properties of NGC 4194[a)]

R.A. (1950.0)	Dec (1950.0)	Type	m_b	Size (blue)	PA	$L_{\rm FIR}$	$\frac{f(60\,\mu{\rm m})}{f(100\,\mu{\rm m})}$	M(HI)	$M_{\rm dyn}$
$12^{\rm h}\ 11^{\rm m}\ 41.22^{\rm s}$	$54^\circ\ 48'\ 16''$[b)]	Pec[c)]	13.0[c)]	$2'.3 \times 1'.6$ [c)]	146[d)]	$8.5 \cdot 10^{10} {\rm L}_\odot$ [e)]	0.97	2.2×10^9 $M_\odot$[f)]	7×10^9 $M_\odot$[g)]

[a)] Other aliases: UGC 07241, Arp 160, Mrk 201, VV 261, I Zw 033
[b)] Radio continuum peak position (Condon et al. (1990)
[c)] from the UGC catalogue (Nilson 1973)
[d)] as measured the bright main body of the optical R-band image (from Mazzarella & Boroson)
[e)] (10 μm - 100 μm), Deutsch & Willner (1987) (for D=39 Mpc)
[f)] Thuan and Martin (1981) (for D=39 Mpc)
[g)] Adopting the inclination $i \approx 40^\circ$ and using Fig. 4, we get $V_{\rm rot}$=115 km s^{-1}. The dynamical mass is $M_{\rm dyn} = 2.3 \times 10^8 (\frac{V_{\rm rot}}{100})^2 (\frac{R}{100})$ M$_\odot$ where $V_{\rm rot}$ is in km s^{-1} and R in pc. For the inner 8″ (1.5 kpc) radius the dynamical mass is $M_{\rm dyn} = 7 \times 10^9$ M$_\odot$. In this unrelaxed system, one should of course use dynamical masses, derived from the assumption of regular rotation, with care.

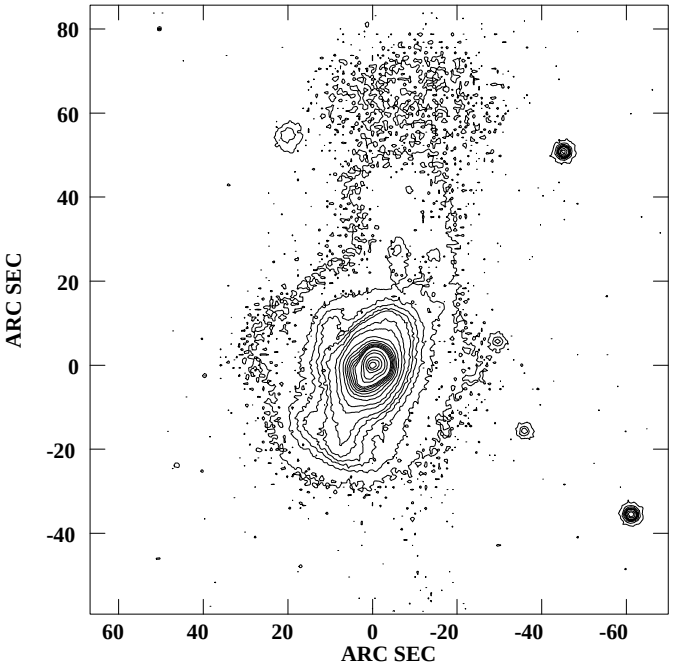

Fig. 1. Contour plot of an R-band CCD image of NGC 4194 (Mazzarella & Boroson 1993). The levels are logarithmic to clearly show the faint structure, such as the northern tidal tail.

to ^{12}CO and not an effect of reduced optical depths in ^{12}CO (e.g. Casoli et al. 1992). However, the moderate optical depth ($\tau \approx 1$) in ^{12}CO 1–0 towards centers of galaxies in general, and ULIRGs in particular, is now a reasonably well established fact (e.g. Aalto et al. 1997; Dahmen et al. 1998; Downes & Solomon 1998).

We have imaged NGC 4194 in the ^{12}CO 1–0 line with OVRO to study the distribution and kinematics of the molecular gas in an HR merger galaxy of moderate luminosity. We have also obtained single dish spectra of the 1–0 transitions of ^{12}CO, ^{13}CO and HCN. The observations are presented in Sect. 2; the results in Sect. 3; the consequences of these findings are discussed in terms of merger history, central gas surface densities and final fate of the molecular gas in Sect. 4.

Table 2. Single dish results

Line	θ (″)	$\int T_{mb}$ (K km s^{-1})
^{12}CO	33	17 ± 2
^{13}CO	34	0.9 ± 0.2[a]
HCN	43	$\lesssim 0.4$[b]

[a] The ^{12}CO/^{13}CO 1–0 intensity ratio is 19 ± 4.
[b] The ^{12}CO/HCN 1–0 intensity ratio is $\gtrsim 25$, corrected for beamsize.

2. Observations

We have obtained high resolution maps of ^{12}CO 1–0 using the Caltech six-element Owens Valley Radio Observatory (OVRO) millimeter array. Two tracks were taken in the low resolution configuration in September and October 1996 and two in the high resolution configuration in December 1996. The naturally weighted synthesized beam size is $2''.5 \times 2''.0$ (472×378 pc for D=39 Mpc) and the beam position angle (BPA) is –66°. The sensitivity of this map is 11 mJy beam^{-1} channel^{-1}, corresponding to 0.19 K channel^{-1}. For a beamsize of $2''.3$ a brightness temperature ($T_{\rm B}$) of 1 K corresponds to 57 mJy at λ=2.6 mm.

For the (naturally weighted) high resolution data only, the beamsize is $2''.0 \times 1''.7$ and BPA is –71°. For a resolution of $1''.85$ a brightness temperature of 1 K corresponds to 36 mJy.

System temperatures were 500–600 K. The quasar 1150+497 was used for phase calibration and Neptune and Uranus for absolute flux calibration. The digital correlator, centered at $V_{\rm LSR} = 2560$ km s^{-1}, provided a total velocity coverage of 1170 km s^{-1}. Data were binned to 4 MHz resolution, corresponding to 10 km s^{-1}, and to construct the map, the resolution was reduced to 20 km s^{-1}.

Single dish spectra of the 1–0 transition of ^{12}CO, ^{13}CO and HCN were obtained toward the center of NGC 4194 with the OSO 20m telescope. The observations were carried out in October 1999, and the system temperatures were typically 400 K for ^{12}CO and ^{13}CO and 200–300 K for HCN. The pointing accuracy was checked on SiO masers and was found to be about 3″. Beam sizes and efficiencies are listed in Table 2, together with the results.

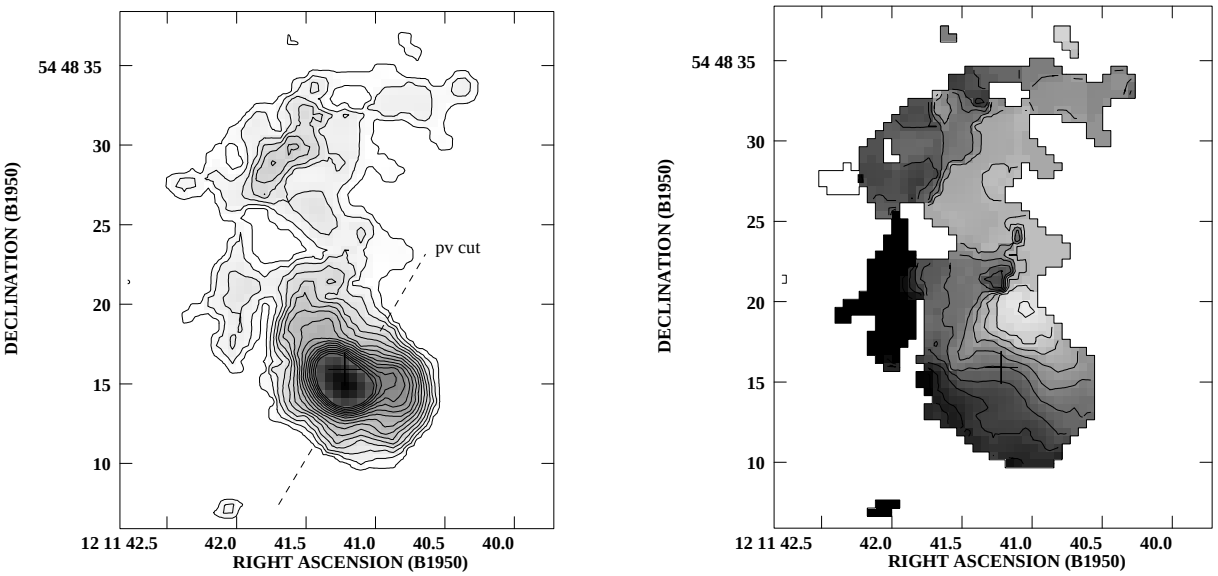

Fig. 2. **a** Integrated intensity of the naturally weighted ^{12}CO map. Contour range is (0.54, 1.6, 2.7, 3.8,..., 31) Jy beam^{-1} km s^{-1}. The grayscale ranges from 0.7 (light) to 27 (dark) Jy beam^{-1} km s^{-1}. The radio continuum position is marked with a cross. The total flux in map is 170 Jy km s^{-1}. The dashed line indicates the location of the position velocity cut in Fig. 6 **b**: The velocity field. Contours range from 2400 to 2640 km s^{-1}, with spacing 24 km s^{-1}. The grayscale ranges from 2400 (light) to 2650 (dark) km s^{-1}

3. Results

3.1. Morpholology and kinematics of the molecular distribution

Integrated intensity: The naturally weighted ^{12}CO emission (Fig. 2a) is distributed on a scale of 30″ (5.7 kpc). The bulk of the emission (67%) is concentrated in an 10″ (1.9 kpc) sized oval structure centered on the optically bright main body. Fainter, patchy emission curves out to the north from the brighter emission.

An overlay of the ^{12}CO distribution on an R-band image (Fig. 3) reveals that the general ^{12}CO morphology is quite different from that of the main optical body of the galaxy. The molecular gas extends from the center to the north-eastern part of the object, and the *major axis of the central ^{12}CO intensity distribution is almost perpendicular to that of the optical body*. The position angle (PA) of the ^{12}CO oval intensity distribution of the bright emission is $\approx 49°$ and the FWHM source size is $4\farcs2 \times 2\farcs5$ The position angle of the optical emission is 146°.

The curved northern ^{12}CO emission reaches into the base of the tidal tail, and some faint emission is also detected near a bright patch (indicated with an arrow in Fig. 3) in the tail itself. In Fig. 3, the ^{12}CO emission appears to be inside of an optical protrusion, or arm, in the east (marked with an arrow in Fig. 3). Armus et al. (1990) describe this feature as a "spur" or a "jet". The blue band image in Arp's Catalog of Peculiar Galaxies (1966) gives instead a strong indication of a foreground eastern dust lane blocking the background emission and creating the impression of a protruding feature separate from the main body. The molecular emission traces the space between the "spur" and the main body which is consistent with the interpretation of a dust lane.

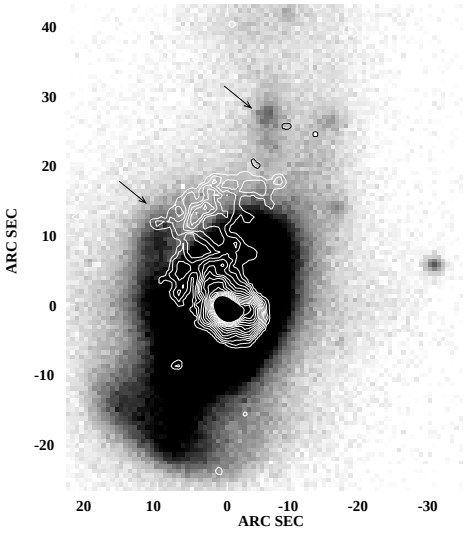

Fig. 3. Overlay of the ^{12}CO contours (white, apart from clouds in the tail marked in black) on a greyscale, overexposed optical R-band image (Mazzarella & Boroson 1993). The left arrow indicates the eastern expansion and the right one points to one of the bright condensations in the northern tidal tail.

The total ^{12}CO flux in NGC 4194 detected by OVRO is 170 Jy km s^{-1} which, for a standard ^{12}CO to H_2 mass conversion factor, translates to 2.3×10^9 M$_\odot$ ($0.92 \times 10^4 S\Delta V D^2$ M$_\odot$ for X = N(H$_2$)/I(^{12}CO) = 2.3×10^{20} cm^{-2} (K km s^{-1})$^{-1}$) of molecular gas. Within calibrational error bars, we recover all of the single dish flux. The peak flux is 27 Jy beam^{-1} km s^{-1} (16% of the total flux) at α: 12$^{\rm h}$ 11$^{\rm m}$ 41.22$^{\rm s}$; δ: 54° 48′ 14.″4. which translates to a molecular mass of 3.8×10^8 M$_\odot$ within a radius of 240 pc. However, we suspect that the conversion factor

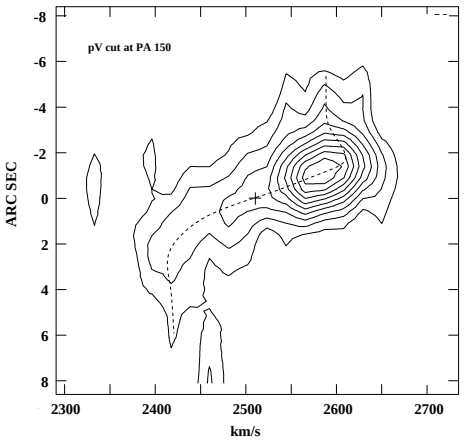

Fig. 4. pV cut at PA 160° across the central ^{12}CO body. The location of the cut is indicated in Fig. 2a. The cross marks the estimated kinematic center of a solid body rotating structure.

overestimates the molecular mass in this system — in particular in the center (see Sect. 4.3.1.).

The velocity field: In Fig. 2b we present the ^{12}CO velocity field which shows the complex dynamics of NGC 4194. Close to the center there seems to be organized rotation of the gas (even though the velocity contours are far from a regular spider diagram) with a position angle of 160° — close to the optical major axis. Thus, the major axis of the rotation of the gas follows the PA of the optical light distribution, rather than the distribution of the ^{12}CO emission. A position-velocity (pV) cut at PA 160° (Fig. 4) indicates a solid-body rotation curve which starts to flatten (or fall) at a radius of 2″ (380 pc). The figure also shows that the ^{12}CO peak is offset from the kinematic center by 1″. The projected rotational velocity is 90 $\mathrm{km\,s^{-1}}$. Thus, for an inclination of 40° (from the optical isophotes) the deprojected rotational velocity is 140 $\mathrm{km\,s^{-1}}$ in the inner 16″ (3 kpc). The systemic velocity at the kinematic center is 2510 $\mathrm{km\,s^{-1}}$.

The extended northern gas in general does not move according to the pattern established in the inner region. The eastern part of the emission is at higher velocities than the western emission and velocity discontinuities can be traced along the curved ridge at the transition between the velocity systems. The highest velocity in the system, 2700 $\mathrm{km\,s^{-1}}$, can be found on the eastern dust lane at δ: 54° 48′ 22″. The velocity of the gas in the eastern dust lane then gradually drops along the lane, until it reaches the tidal tail where the velocity of the gas clumps is 2580 $\mathrm{km\,s^{-1}}$.

The Dispersion Map: Fig. 5 displays the dispersion map with a few selected spectra. The one dimensional dispersion is quite moderate, $\sigma_{1\mathrm{d}} \lesssim 10\,\mathrm{km\,s^{-1}}$ in large parts of the galaxy. Regions of high dispersion are found where the velocity field shows discontinuities or irregularities, and the sample spectra reveal that here the enhanced velocity dispersion is caused by multiple spectral features rather than genuinely broad lines. The velocity shifts between the narrow peaks is 150–200 $\mathrm{km\,s^{-1}}$, i.e. the typical rotational velocity of a spiral galaxy. There is also a continuous curved region of elevated dispersion (i.e. multiple spectra) in the center of the map. Even the width of the spectrum at the intensity peak is quite low (lower panel, right hand side) with $\sigma_{1\mathrm{d}} = 50\,\mathrm{km\,s^{-1}}$, which is narrow for the center of a merging system.

Channel Maps: Dividing the emission into three velocity bins, (2380–2485 $\mathrm{km\,s^{-1}}$), (2506–2570 $\mathrm{km\,s^{-1}}$), (2590–2720 $\mathrm{km\,s^{-1}}$), (Figs. 6a,b,c) shows the emission being distributed in long, arm-like features of quite different appearence in the three bins. The low and high velocity bins were chosen to include each one of the two features seen in the double peaked spectra (e.g. middle right panel in Fig. 5). The middle bin includes emission at intermediate velocities near the systemic value.

The low velocity map (Fig. 6a) shows a patchy distribution extending over 20″ to the north-south. Closer to the center, brighter emission curves 5″ in the east-west direction.

At mid-velocities (Fig. 6b), the distribution is dominated by a striking, elongated curved shape, approximately 15″ (2.8 kpc) in length. This structure is the main cause of the discrepancy between the ^{12}CO emission distribution and the R-band light distribution. It traces a central prominent dust lane. To show this, we have overlayed the mid-velocity ^{12}CO emission on an archival HST image in Fig. 7. Another, fainter, 20″ (3.8 kpc) long curved structure is found in the north. This feature may be a continuation of the central dust lane and the gap between them a depression in the ^{12}CO brightness.

The high velocity emission bin (Fig. 6c) shows a bright peak in the center with a source size of $2\farcs5 \times 1\farcs8$. A prominent, narrow curved feature stretches out to the north-east, (20″ to the north) and follows most of the eastern obscuring dust lane seen in Arp's B-band image. We suggest the northern, curved feature in the mid-velocity bin is the continuation of this curve. As mentioned above, the central dust lane may connect to this feature as well. In Fig. 6d the features in the three velocity bins are marked with dashed lines.

3.1.1. The high resolution map — a close-up on the center

For a closer look at the structure of emission in the inner 10″, we selected the high resolution data only, and thus increased the resolution to 1.″7 (but lost some sensitivity and uv-coverage). The integrated intensity map (Fig. 8a) of the inner region consists of 5 peaks, a, b, c, d and e (Table 3) and extended emission surrounding them. The total flux of the inner $10'' \times 10''$ is 64 Jy km s^{-1}. The brightest peak, a (17 Jy $\mathrm{km\,s^{-1}}$ beam^{-1}), is at the same position as in the lower resolution map, i.e. close to the radio continuum peak, but shifted to the south by 1.″5 (280 pc). Feature a has a size of $1\farcs8 \times 1\farcs3$ and a position angle of 45°. The fitted FWHM sizes of features a–e are typically 200–400 pc, which is comparable to the sizes of Giant Molecular Associations (GMAs) found in other galaxies. Features b and c can be identified with knots in the Hα distribution (Armus et al. (1990)). The peak intensity in the high resolution map is 200 mJy, which corresponds to 5.4 K.

Fig. 9 is an overlay of the integrated high resolution ^{12}CO emission on an archival HST image (enhanced to show the dust

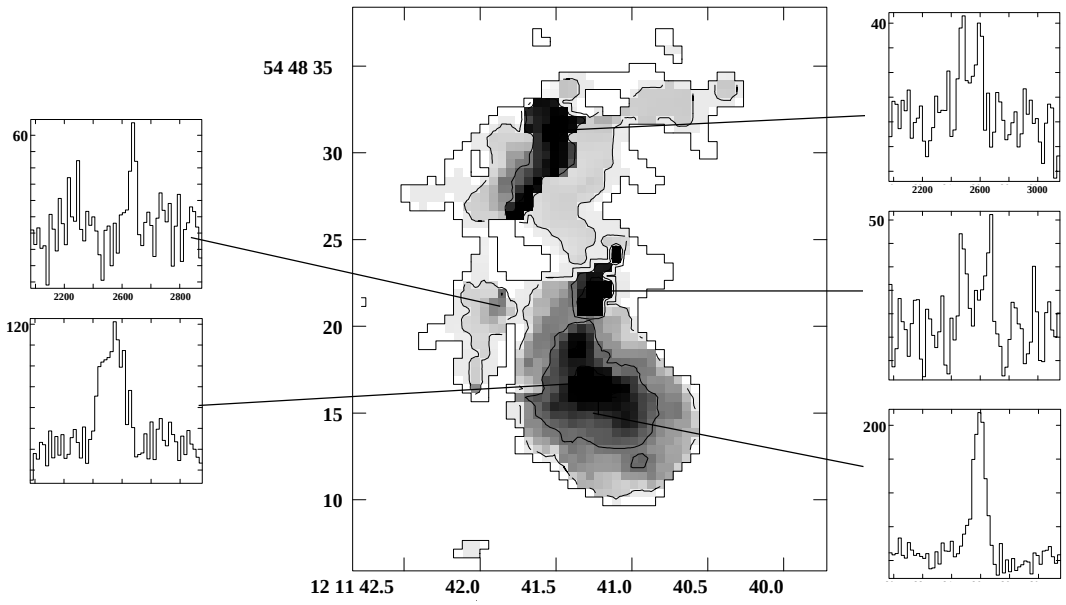

Fig. 5. Dispersion map with sample spectra. The contours are (12, 36, 60) $\mathrm{km\,s^{-1}}$ and the grayscale ranges from 6 (light) to 60 (dark) $\mathrm{km\,s^{-1}}$. The sample spectra are selected to show regions of multiple spectral features and the central region.

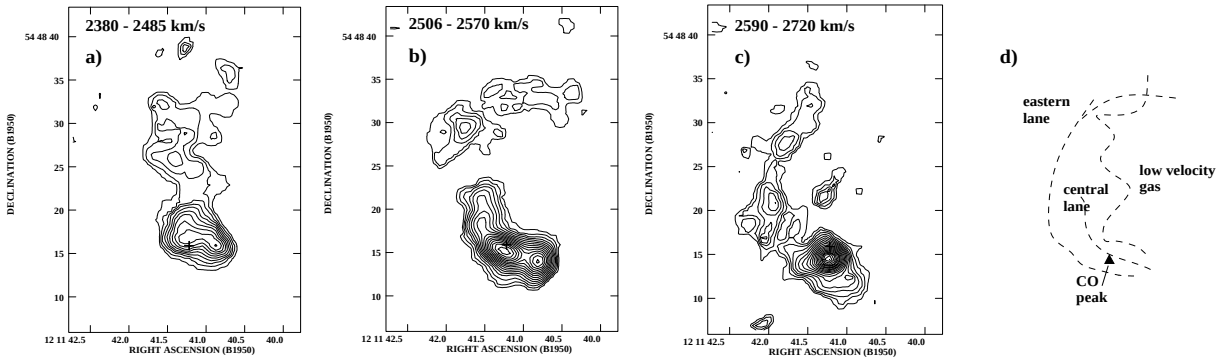

Fig. 6a–d. The left panel **a** shows the integrated intensity (naturally weighted ^{12}CO map) in the lower part of the velocity range (2380–2485 $\mathrm{km\,s^{-1}}$), panel **b** shows the central part of the velocity range (2506–2570 $\mathrm{km\,s^{-1}}$), and panel **c** shows the highest velocities (2590–2720 $\mathrm{km\,s^{-1}}$). The dashed lines indicate the position of the central dust lane from the mid velocity panel. Contours are (0.7, 1.4, 2.1, 2.8... 14) Jy beam^{-1} $\mathrm{km\,s^{-1}}$. The cross marks the radio continuum position. The right panel **d** is a sketch where the features from the three velocity bins are indicated with dashed lines.

lane, same as Fig. 5). The peaks a, b, d and e all lie on the central dust lane.

The velocity field (Fig. 8b) is slightly more twisted than in the lower resolution map and covers the same velocity range. Features d and c are causing twists in the velocity field because they are at too low velocities to fit a spider diagram. The maximum dispersion (100 $\mathrm{km\,s^{-1}}$) in Fig. 8c does not occur in a, but in an elongated (east-west) region located north of the ^{12}CO peak, close to feature b. This is caused by the crossing of the dust lane, i.e. by a superposition of multiple spectral features.

Fig. 10 shows an overlay of the ^{12}CO emission on the 1.49 GHz radio continuum structure (Condon et al. 1990). There is a rough agreement between the CO and the radio-continuum distribution which seems to break down at smaller scales (i.e. less than 1 kpc). The ^{12}CO peak (feature a), for example, is located $1''$ south of the radio continuum peak. There is an arm-like structure curving from the center to the west which has a ^{12}CO counterpart in feature c. The one ^{12}CO feature entirely lacking in the continuum distribution is e in the north. Comparisons between radio continuum and CO distributions in starburst galaxies often show a correlation between the two distributions (e.g. Yun et al. 1994, Bajaja et al. 1995). This effect is often attributed to cosmic ray heating of the molecular gas (e.g. Adler et al. 1991; Allen 1992). We will discuss this correlation further in Sect. 4.2.

3.2. Single dish results

Results are presented in Table 2 and ^{12}CO, ^{13}CO spectra in Fig. 12 (HCN was not detected, and its spectrum is not shown). The ^{12}CO flux detected by OVRO is, within calibrational error bars, the same as measured by the OSO 20m telescope, which

Table 3. Central emission peaks

Peak	R.A. (1950.0)	Dec (1950.0)	Peak Intensity	Size (FWHM)	V_c ($\mathrm{km\,s^{-1}}$)	Notes
	(1950.0)	(1950.0)	($\mathrm{Jy\,km\,s^{-1}\ beam^{-1}}$)	$''$	($\mathrm{km\,s^{-1}}$)	
a	$12^h\ 11^m\ 41.22^s$	$54°\ 48'\ 14.''4$	17	$1.''5$	2592	^{12}CO peak
b	$12^h\ 11^m\ 41.28^s$	$54°\ 48'\ 15.''9$	13	$2.''5 \times 0.''8$	2531	on dust lane[a]; Hα knot
c	$12^h\ 11^m\ 40.82^s$	$54°\ 48'\ 15.''4$	8.6	$1.''7 \times 0.''5$	2496	Hα knot
d	$12^h\ 11^m\ 40.75^s$	$54°\ 48'\ 13.''9$	6.9	$1.''8 \times 0.''7$	2539	on dust lane
e	$12^h\ 11^m\ 41.57^s$	$54°\ 48'\ 18.''4$	4.6	$2.''4$	2563	on dust lane

[a] Double spectrum: peaks at 2464 $\mathrm{km\,s^{-1}}$ and 2549 $\mathrm{km\,s^{-1}}$ (main)

is approximately 60% more than the flux Devereux et al. (1994) find with the FCRAO 14m telescope.

We note that the integrated ^{12}CO/^{13}CO intensity ratio we find is lower, ≈ 20, than previously reported by Casoli et al. (1992), ≈ 55, although their error bar of ± 22 includes our measurement. Our result means that NGC 4194 is not an extreme HR merger and ^{13}CO 1–0 is quite detectable, even if the ratio is clearly above what is usually found for starburst galaxies. There is a hint of a line shape difference in the ^{12}CO and ^{13}CO lines with an extra narrow component at lower velocities in the ^{13}CO spectrum. The signal to noise ratio in the ^{13}CO spectrum is too low to warrant further speculation on this matter here, but a high resolution ^{13}CO image may reveal interesting excitation changes across the galaxy, as has already been shown for the merger starburst system Arp 299 (Aalto et al. 1997; Casoli et al. 1999). The HCN emission is at least as faint as the ^{13}CO emission with the ^{12}CO/HCN intensity ratio $\gtrsim 25$. In comparison to other FIR luminous galaxies (e.g. Solomon et al. 1992) the HCN is relatively faint.

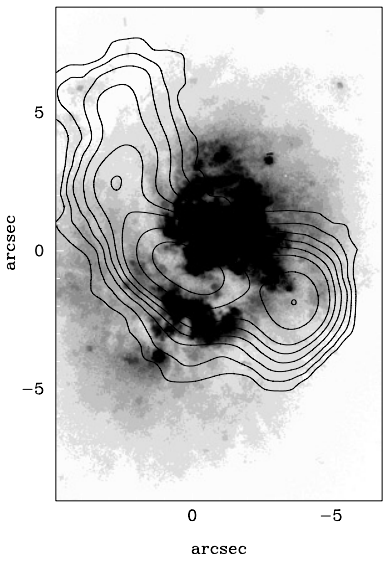

Fig. 7. Contours of the mid-velocity (2506–2570 $\mathrm{km\,s^{-1}}$) ^{12}CO emission overlaid on an archival HST WFPC2 image which shows the ^{12}CO emission tracing a prominent central dust lane.

4. Discussion

4.1. Merger timescale and ^{12}CO morphology

4.1.1. The Medusa as a major disk-disk merger

Joseph & Wright (1985) suggested that NGC 4194 is a collision between two disk galaxies and put it fairly late in a merger sequence: after Arp 220 and before NGC 3310. They used the apparent diffuseness of the tidal tail and the coalesced optical main body as principal arguments for this placement in the evolutionary scheme.

However, despite the suggested advanced stage of the NGC 4194 merger, the molecular gas structure is complex and distributed on a scale of several kpc. In the late stages of a merger, simulations suggest that the bulk of the molecular gas would have sunk to the inner 200 pc of the merger, regardless of the previous morphology/orientation of the precursor galaxies (e.g. Barnes & Hernquist 1996). The corresponding size scale for NGC 4194 is an order of magnitude greater than that. The funneling of molecular gas toward the center of NGC 4194 has been less effective than for ULIRGs, such as Arp 220 or NGC 6240, which is interesting since both these mergers appear younger than NGC 4194. Apart from the ULIRGs being more luminous by factors of at least 10, they also have broader line widths, and deeper potentials. If NGC 4194 is the result of the merger of two disk galaxies of comparable mass, i.e. a 'major merger', either the merger is less advanced than previously thought, or the intrinsic and/or orbital properties of the NGC 4194 progenitors are, after all, important factors.

One can use the presence and separation of a double nucleus as an indication of merger age. In NGC 4194 there is no obvious sign of another nucleus, but there is a fairly bright extension to the south of the radio continuum emission, which is the location of the ^{12}CO peak, a. If a is another nucleus in the merging system, then the projected separation between them is $1.''5$, or 280 pc. However, the non-compact appearance (and lower luminosity) of a indicates instead that it is a bright star forming region rather than a second nucleus, in which case the upper limit of the nuclear separation becomes even more strict. It is perhaps also possible that merger orientation hides the second nucleus behind the first one, but this should be a rather unlikely scenario.

We find it difficult to reconcile the extended, unrelaxed appearance of the molecular gas distribution with a major merger scenario where the lack of a double nucleus indicates a very

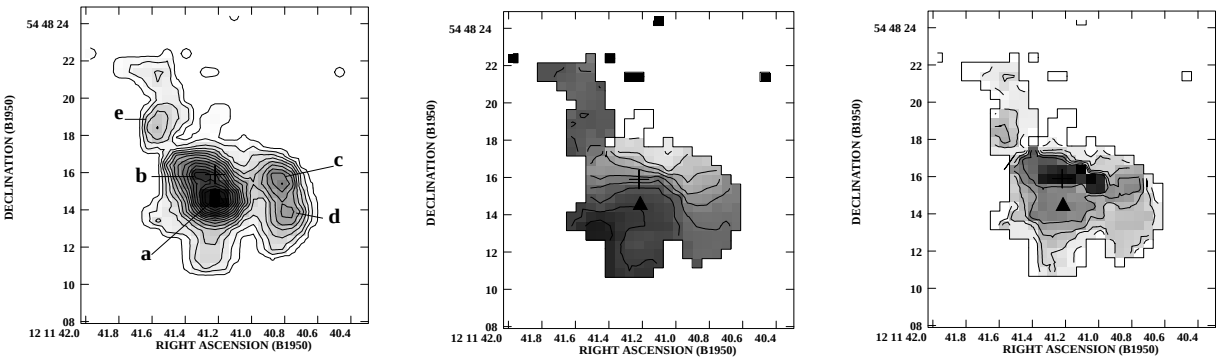

Fig. 8. **a** Map of total integrated intensity for the high resolution data only showing the inner region of NGC 4194. Contours are (0.5, 1.5, 3.5,...) Jy beam^{-1} km s^{-1}. The peak flux is 17 Jy beam^{-1} km s^{-1}. The intensity peaks are designated a to e with falling peak intensity. The grayscale ranges from 1 (light) to 16 (dark) Jy beam^{-1} km s^{-1}. **b** The high resolution velocity field. Contours and grayscale are the same as in Fig. 2b. The position of the ^{12}CO peak a is indicated with a black triangle. **c** High resolution dispersion map. The position of the ^{12}CO peak a is indicated with a black triangle.

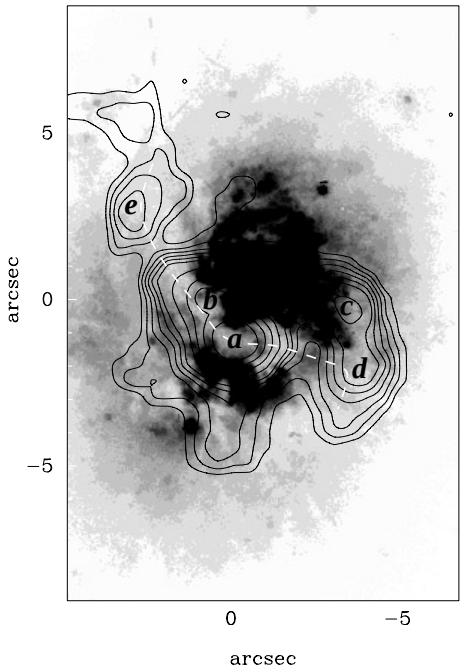

Fig. 9. Overlay of the integrated high resolution ^{12}CO emission in contours on an archival HST image (same as Fig. 5). The central dust lane is indicated as a white, dashed line, and most of the ^{12}CO peaks (a, b, d, e) lie on this lane. The ^{12}CO peaks are indicated with their corresponding letters.

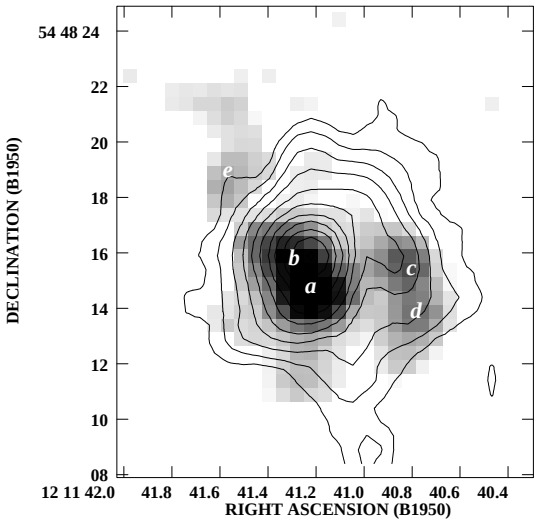

Fig. 10. Overlay of the radio 1.49 GHz radio continuum (Condon et al. 1990) in contours on the high resolution ^{12}CO emission in grayscale. The ^{12}CO features are labeled with their corresponding letter. The contours are logarthimically spaced, as in Condon et al..

advanced merger. Together with the morphological appearance of the Medusa, this lead us to suggest another merger scenario:

4.1.2. The Medusa as a young shell-galaxy

The southern sharp, curved feature seen in the optical image may well be a shell in its early stages of formation, thus raising questions on whether an elliptical/early-type galaxy was one of the progenitors. The total molecular mass of 2×10^9 M$_\odot$ is indeed less than what one would expect from the collision of two gas-rich disks.

Quinn (1984) found that shells can form through "phase-wrapping" of dynamically cold disk material in a rigid, spherical potential. The similarity between the overall Medusa morphology and simulations of a radial, planar collision between a disk galaxy and a more massive spherical, is striking (e.g. Quinn 1984, Fig. 1 timestep 6; Kojima & Noguchi (KN) 1997, Fig. 4a timestep 4.7, 6.2). The first shell is forming on the opposite side of the single, broad tidal tail creating an almost "cometary" structure. Although, we note that the implied molecular mass of NGC 4194 suggests that the disk galaxy involved was more massive than a dwarf — which is often assumed in the simulations.

KN also simulated the behaviour of the gaseous component during the encounter and found that the gas becomes scattered much like the disk stars. This is in sharp contrast to the models of Weil & Hernquist (WH)(1993) who instead conclude that

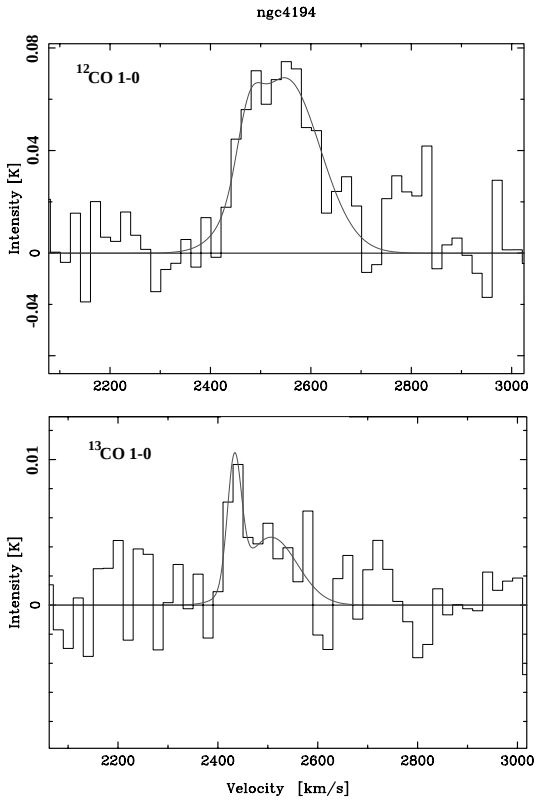

Fig. 11. The OSO 20m telescope single dish spectrum of ^{12}CO (upper panel) and ^{13}CO (lower panel). The intensity scale is in $T_{\rm mb}$.

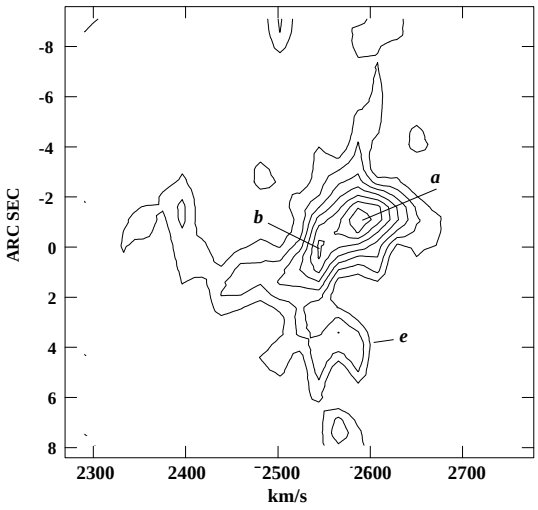

Fig. 12. position velocity cut along the central dust lane, from e to a.

the gas from the disk galaxy quickly sinks to the center of the merger. This also leads to different views on the occurence of starbursts in these encounters. In the KN approach, the scattering of gas clouds prevents star formation, while WH suggest that starbursts are likely to occur in the central gas concentration. In the WH model the shells are expected to be gas-poor because of the separation between gas and stars. The difference between the KN and WH models is largely caused by their ISM represenation: KN using sticky particles and WH a hydrodynamical model.

Now, if we adopt the notion that NGC 4194 is indeed a radial collision between a spiral and a more massive, gas-poor spherical (i.e. an unequal mass, or 'minor' merger), we can make the following observations: No molecular gas is detected in the southern shell in accordance with the WH model, but perhaps more sensitive observations can find gas here. Both HI and CO has been detected in the shells of Centaurus A (Schiminovich et al. 1994; Charmandaris, Combes & van der Hulst 2000). The molecular gas is not scattered all over the system, nor can all of it be found in the very inner region. The distribution is somewhere in between the two models, and the gas in the inner region seems to be going through a starburst on a fairly large scale (see Sect. 4.2). The multiple spectral components may reflect gas on different orbits and in different stages of its dance around the center of the elliptical. The velocity shift between the two components is roughly the same as the typical rotational velocity for a spiral galaxy. Thus the existence of two spectral components does not necessarily imply that the molecular gas is coming from two different progenitor galaxies. For both the major and minor merger models, however, the presence of two spectral components suggests that the gas has some time to go before it reaches relaxation.

However, the elliptical-spiral model leaves us with (at least) two quesions: 1) where is the massive elliptical? 2) what is the significance of the (very) faint tail to the south (which can only be seen in deep images)? The first question can better be answered once there is a near infrared K-band image that can see through the dust lanes and dust enshrouded starburst currently hiding the center. The southern tail is very diffuse, and may be a remnant of an earlier interaction. Its significance can be better judged by sensitive HI observations.

We have made a search through galaxy morphology catalogues looking for Medusa-like mergers. We found three more objects with similar morphology (i.e. one prominent tidal tail and on the opposite side of the galaxy a sharp curved feature): ESO 240-G01, NGC 7135 and NGC 5018. So, the Medusa morphology is not unique, but fairly rare, which could be an effect of the rather short timescales involved in the radial encounters. The Medusa still stands out among these objects because of its bright FIR emission and hot dust. Perhaps the Medusa is in a short-lived stage of intense star formation that will consume a large fraction of the molecular gas, leaving the galaxy to look more like NGC 7135 once the burst is over.

4.2. The starburst

The starburst of NGC 4194 is extended on a scale of ≈ 2 kpc (e.g. Wynn-Williams & Becklin 1993; Armus et al. 1990) where also 67% of the total ^{12}CO emission can be found. We suggest that overall solid body rotation of the inner gas (see Fig. 4) provided a dynamical environment favourable to a burst of star formation (Keel 1993). At least 90% of the FIR luminosity can be attributed to a burst of star formation (Prestwich et al. 1994; Rowan-Robinson & Crawford 1989) and the high $f(60\,\mu\mathrm{m})/f(100\,\mu\mathrm{m})$

flux ratio (Table 1) indicates that the starburst is heating the dust clouds to high temperatures.

Suchkov et al. 1993 argue that the correlation between CO and radio continuum distributions found in galaxies is an effect of cosmic ray heating of the molecular gas. They suggest that changing values in the ratio of CO and radio continuum intensity are indicators of the starburst age, with young starbursts having a higher value than old bursts since the cosmic rays are more confined to the molecular layer if the burst is young. In this model, the (low energy) cosmic rays originate in supernove remnants (SNRs). Their electron component is responsible for the radio continuum emission at cm wavelengths, while their proton component heats the gas. This provides a natural explanation for the rough correlation between continuum and molecular line emission – both are tied to star formation activity. This relation is, however, also expected if the (largely non-thermal) continuum emission simply traces SNRs and UV radiation from massive stars plays the major role in the heating of the dust and gas.

It is of course also possible to find molecular gas without a strong radio continuum counterpart if the gas is quiescent and star formation has not (yet) set in. The molecular peak e in Fig. 10 may be an example for such a region.

Bonatto et al. (1999) compare NGC 4194 with the starburst merger NGC 3256. Their population synthesis results suggest that both galaxies have very similar stellar populations. Starbursts occured both at intermediate (1–2 Gyr) and young ages. NGC 3256 also has a kpc scale starburst (Graham et al. 1984) and is an HR merger with relatively faint ^{13}CO 1–0 emission (e.g. Aalto et al. 1991a) and hot dust.

4.3. The central gas surface densities and the molecular line ratios

The ^{12}CO surface brightness of NGC 4194 is lower by an order of magnitude compared to other HR mergers such as Arp 220 and Mrk 231. The average gas surface density for the extended starburst region of NGC 4194 is 500 — 1000 $M_\odot$ pc^{-2}, i.e. more than an order of magnitude below the surface density found in ULIRGs for the same CO–H_2 conversion factor (e.g. Bryant & Scoville 1999). Addressing the question of the reason for the high $\mathcal{R}$ posed in the introduction, we therefore conclude that the turbulent, extreme high pressure scenario for compact nuclear starburst regions (Aalto et al. 1995) is not well suited for explaining the unusual molecular line ratio of NGC 4194. Instead, we adopt a similar explanation as for NGC 3256: high gas temperatures depopulating the lower levels coupled with a disrupted and fragmented ISM (Aalto et al. 1991). One way of testing this scenario is to measure the ^{12}CO/^{13}CO intensity ratio for higher rotational transitions, and to obtain high resolution images of ^{12}CO and ^{13}CO like those for the Arp 299 merger. We can also conclude that NGC 4194 is the exception to the general trend of increasing central concentration of the molecular cloud distribution with increasing $f(60\,\mu\mathrm{m})/f(100\,\mu\mathrm{m})$ flux ratio (Bryant 1997). A study of the intrinsic properties of compact and kpc scale HR galaxies is underway (Aalto et al., in preparation).

The star formation rate (SFR) in NGC 4194 has been estimated to be $\approx$40 $M_\odot$ yr^{-1} (Storchi-Bergmann et al. 1994), based on Hα emission. This is not much lower than the estimate for the HCN-bright ULIRG Arp 220, $\approx$110 $M_\odot$ yr^{-1} for Arp 220 (Smith et al. 1998). Assuming a similar conversion factor for both galaxies, Arp 220 has about an order of magnitude more molecular gas in its central region. This would imply a considerably higher star formation efficiency in NGC 4194. However, the SFR for Arp 220 was determined based on its FIR luminosity (see Scoville & Soifer 1991 for the method). Thus, the estimates are done at different wavelenghts and should be viewed with some caution. Indeed, if the SFR of NGC 4194 is determined using the FIR luminosity, the result is much lower (6–7 $M_\odot$ yr^{-1}), resulting in star formation efficiencies for NGC 4194 and Arp 220 that are comparable.

The ratio of L_{FIR}/L_{CO} ratio is indeed similar in both galaxies implying that both starbursts are equally efficient in producing IR photons per unit molecular mass (again assuming that CO traces mass in roughly the same way in both objects).

Even if the star formation efficiencies and the L_{FIR}/L_{CO} are similar, there may be significant differences in the star formation properties of moderate luminosity mergers and ULIRGs, since the ISM in the two types of galaxies has a different structure. The starburst of NGC 4194 takes place in a low pressure environment compared to the starbursts at the heart of ULIRGs. The lower gas pressure results in a lower mass fraction of dense clumps and may allow destructive UV photons to penetrate further into the molecular clouds, where they can heat the dust and dissociate the molecules. Then, the young, massive stars in NGC 4194 would have a larger impact on the surrounding gas, disrupting it more effciently. This may also account for the relatively high brightness in Hα and the hot dust. NGC 4194 has near solar metallicity, so the apparently efficient heating of the dust cannot be explained by a gas-to-dust ratio that is unusually low (e.g. Bonatto et al. 1999; Storchi-Bergmann et al. 1994).

4.4. The fate of the molecular gas

The elevated ^{12}CO/^{13}CO 1–0 molecular line ratio together with the IR properties indicate that the molecular gas is being strongly affected by the newborn stellar population. The estimated star formation rate of NGC 4194 is about 40 $M_\odot$ yr^{-1} which, if it continues, will have consumed the available gas in the center within 40 million years. The unusual molecular cloud properties may well be an indication that the standard conversion factor is inapplicable, so the real gas consumption time scale may be lower. The cloud properties will likely be quite similar to those in the NGC 3256 model (Aalto et al. 1991a) where the kinetic gas temperatures are found to be close to 100 K and the clouds are quite small, a few pc in size. Such a molecular ISM will radiate more brightly per unit mass than the cool disk clouds for which the conversion factor is calibrated. Experience from the NGC 3256 model leads us to suggest that the real molecular

mass in the starburst region may be a factor of ≈5 lower than the mass based on the 'standard' conversion factor.

If all of the gas is to be consumed, also the gas at higher galactic radii needs to be transported to the center. The morphology of the central dust lane with respect to the ^{12}CO peak is very suggestive of gas transport to the center. A position-velocity cut (Fig. 12) along the central dust lane, from e to a, shows that the gas on the dust lane may be moving continuously into the ^{12}CO peak a. On both sides of a along the dust lane the velocities are lower by $50\,\mathrm{km\,s^{-1}}$ than in a, which could imply that gas is flowing into a. It is of course also possible that a does not lie on the dust lane, but further to the core of the galaxy, in which case this may simply be a projection effect. Then again, the fact that a is offset from the kinematic center argues against this last possibility. There are interesting morphological features on the dust lane just east and west of a where it seems to flare out into a triangular shape, and darken (brighten in the negative figures). From Fig. 12 it is also clear that at the position of b the emission splits into a brighter part at higher velocities and fainter emission at lower velocities.

The final appearance of NGC 4194 may well be that of an elliptical with shells and a remaining minor axis dust lane.

5. Summary

We have obtained a high resolution map of the Medusa merger, NGC 4194, in the ^{12}CO 1–0 line. The main conclusions we draw from this map and single dish ^{12}CO, ^{13}CO and HCN observations are as follows:

1. The molecular distribution in NGC 4194 is extended over almost 5 kpc. Thus, this moderate luminosity merger shows clear morphological differences to typical ULIRGs, where an FIR luminosity higher by an order of magnitude usually goes along with a very compact molecular distribution on a scale of $\lesssim$ 1kpc.
2. The structure revealed by our map is complex, consisting of a rotating central concentration, low level emission extending north almost into the base of the tidal tail and very prominent arcs and filaments that can be identified with two dust lanes visible in the optical.
3. Along the central dust lane, we can identify several clumps that may be Giant Molecular Associations (GMAs). Some of these GMAs are positionally coincident with radio continuum features. However the strongest molecular concentration visible in ^{12}CO is offset from the radio continuum peak. This peak may represent a second pre-merger nucleus in the system or – more likely – a region of exceptionally strong gas concentration and star formation.
4. NGC 4194 is clearly detected in a single dish ^{13}CO spectrum. Thus, it has a high but not extreme ^{12}CO/^{13}CO line intensity ratio of $\sim$ 20. The extent of the molecular distribution and the relative central surface density of the gas indicate that the physical mechanism causing the high $\mathcal{R}$ is different in NGC 4194 from ULIRGs with high values of $\mathcal{R}$. We suggest that a scenario with small clouds having high kinetic temperatures may account for the high $\mathcal{R}$ found in NGC 4194, but cannot exclude that diffuse gas may also play a role.
5. The non-detection of the high density tracer HCN indicates that the amount of dense gas in NGC 4194 is lower than in ULIRGs. However, the star formation efficiency may be nearly the same, with a gas consumption time of less than 40 million years. Alternatively, massive young stars may have a higher impact on the fragmented ISM we suggest for NGC 4194.
6. It is likely that gas is at present flowing along the dust lanes toward the nucleus. However, the extended molecular distribution is at odds with the classification of NGC 4194 as an advanced major merger. The two properties can only be reconciled if the gas flow to the center of the system was inefficient compared to ULIRGs. Alternatively, NGC 4194 can be interpreted as an emerging shell galaxy resulting from a merger beween an early type and a spiral galaxy. Comparing simulations of such encounters with the morphology of NGC 4194 lead us to favour this latter interpretation of the Medusa merger history.

To further our understanding of the merger history of NGC 4194, the system needs to be mapped in more molecular transitions as well as H I and Hα. It represents a class of little studied moderate luminosity mergers. More generally, knowledge about the parameters that govern the extent and efficiency of the starburst resulting from a merger and its connection to the progenitors can only be gained if the moderate luminosity systems are investigated along with the high luminosity ones. If galaxy formation at high z happened through mergers, it is essential to understand the differences between different types of mergers in the local universe, where the systems can be resolved with present techniques.

Acknowledgements. Many thanks to Peter Bryant for his help in initiating this study. We thank J. Mazzarella for generously sharing his R-band image of NGC 4194 with us. We are thankful for the useful suggestions by an anonymous referee. This research has made use of the NASA/IPAC Extragalactic Database (NED) which is operated by the Jet Propulsion Laboratory, California Institute of Technology, under contract with the National Aeronautics and Space Administration. The OVRO mm-array is supported in part by NSF grant AST 9314079, and by the K.T. and E.L. Norris Foundation.

References

Aalto S., Black J.H., Booth R.S., Johansson L.E.B., 1991a, A&A 247, 291
Aalto S., Black J.H., Johansson L.E.B., Booth R.S., 1991b, A&A 249, 323
Aalto S., Booth R.S., Black J.H., Johansson L.E.B., 1995, A&A 300, 369
Aalto S., Radford S.J.E., Scoville N.Z., Sargent A.I., 1997, ApJ 475, L107
Adler D.S., Lo K.Y., Allen R.J., 1991, ApJ 382, 475
Allen R.J., 1992, ApJ 399, 573
Armus L., Heckman T.M., Miley G.K., 1990, ApJ 364, 471
Arp H., 1966, ApJS 14, 1
Bajaja E., Wielebinski R., Reuter H.-P., et al., 1995, A&AS 114, 147

Barnes J.E., Hernquist L., 1996, ApJ 471, 115
Bonatto C., Bica E., Pastoriza M.G., Alloin D., 1999, A&A 343, 100
Bryant P., 1997, Ph.D. Thesis, California Institute of Technology
Bryant P., Scoville N.Z., 1996, ApJ 457, 678
Bryant P., Scoville N.Z., 1999, AJ 117, 2632
Casoli F., Dupraz C., Combes F., 1992, A&A 264, 55
Casoli F., Willaime M.-C., Viallefond F., Gerin M., 1999, A&A 346, 663
Charmandaris V., Combes F., van der Hulst J.M., 2000, A&A 356, 1
Condon J.J., Helou G., Sanders D.B., Soifer B.T., 1990, ApJS 73, 359
Dahmen G., Hüttemeister S., Wilson T.L., Mauersberger R., 1998, A&A 331, 959
Deutsch L.K., Willner S.P., 1987, ApJS 63, 803
Devereux N., Taniguchi Y., Sanders D.B., et al., 1994, AJ 107, 2006
Downes D., Solomon P., 1998, ApJ 507, 615
Graham J.R., Wright G.S., Meikle W.P.S., Joseph R.D., Bode M.F., 1984, Nat 310, 213
Joseph R.D., Wright G.S., 1985, MNRAS 214, 87
Keel W.C., 1993, AJ 106,177
Kojima M., Noguchi M., 1997, ApJ 481, 132 (KN)
Mazzarella J.M., Boroson T.A., 1993, ApJS 85, 27
Nilson P., 1973, Uppsala General Catalogue of Galaxies. Acta Universitatis Upsaliensis, Nova Regiae Societatis Upsaliensis, Series V:A, Vol. 1
Prestwich A.H., Joseph R.D., Wright G.S., 1994, ApJ 422, 73
Quinn P.J., 1984, ApJ 279, 596
Rowan-Robinson M., Crawford J., 1989, MNRAS 238, 523
Scoville N.Z., Sanders D.B., Sargent A.I., Soifer B.T., Tinney C.G., 1989, ApJ 366, L5
Scoville, N.Z., Soifer, B.T., 1991, In: Leitherer C., Walborn N., Heckman T., Norman C. (eds.) Massive Stars in Starbursts. Cambridge University Press, Cambridge, p. 233
Schiminovich D., van Gorkom J.H., van der Hulst J.M., Kasow S., 1994, ApJ 423, 101
Smith H.E., Lonsdale C.J., Diamond P.J., 1998, ApJ 493, L17
Solomon P.M., Downes D., Radford S.J.E., 1992, ApJ 387, L55
Storchi-Bergmann T., Calzetti D., Kinney A., 1994, ApJ 429, 572
Thuan T.X., Martin, 1981, ApJ 247,823
Yun M.S., Scoville N.Z., 1995, ApJ 451, L45
Weil M.L., Hernquist L., 1993, ApJ 405, 142 (WH)
Wynn-Williams C.G., Becklin E.E., 1993, ApJ 412, 535